Rotating the Color Glass Condensate: Stabilizing High-Energy Evolution at NLO

Piotr Korcyl

in collaboration with R. Boussarie, P. Caucal, Y. Mehtar-Tani.

33rd International Workshop on Deep Inelastic Scattering and Related Subjects (DIS2026)
4-8 May 2026

NATIONAL SCIENCE CENTRE POLAND This work is supported by NCN grant nr 2022/46/E/ST2/00346.

NLO approach to BK

Theory contribution: R. Boussarie, P. Caucal, Y. Mehtar-Tani
2509.20236 [hep-ph]

Numerical implementation: R. Boussarie, P. Caucal, P. Korcyl,
Y. Mehtar-Tani
2511.07509 [hep-ph]

NLO approach to BK

Obstacles at NLO

- instabilities observed in NLO BFKL [Salam, Ciafaloni, Colferai (1998)]
- negative cross-section in forward hadron production in pA collisions [Shi, Wang, Wei, Xiao (2021); Liu, Xie, Kang, Liu (2022)]
- wrong sign of Sudakov logarithms [Caucal, Salazar, Schenke, Venugopalan (2022); Taels, Altinouk, Beuf, Marquet (2022)]
- modification of the LO BK kernel to resum double logarithms [Beuf (2014)]
- change of rapidity variable [Ducloue, Iancu, Mueller, Soyez, Triantafyllopoulos (2015-2019)]

Rotation

$$\sigma(x,Q^2) = \sum_{n=2}^{\infty} \int_{x_i} H^{(n)}(Q^2, \{x_i\}_{i=1}^n, \zeta/s) \times \left(S^{(n)}(\{x_i\}_{i=1}^n, \zeta) - 1 \right)$$

where ζ is the factorization scale in rapidity space and $S^n \sim \langle U_1 U_2 \dots U_n \rangle$ is the correlator of n Wilson lines,

$$S^n \equiv (x_1 x_3 \dots x_n x_2 | S) = S_{13} S_{34} \dots S_{n2}.$$

With this notation, the LO BK equation reads

$$\frac{\partial}{\partial \ln \zeta}(2|S) = \bar{\alpha} \Big[(2|K|3)(3|S) + (2|K|2)(2|S) \Big]$$

and the solution exponentiates

$$|S(\zeta)) = e^{-\bar{\alpha} K(\bar{\alpha}) \ln \frac{\zeta}{\zeta_0}} |S(\zeta_0)).$$

Rotation

A scheme transformation can be achieved by a nonunitary operator

$$|\bar{S}(\zeta,\mu^2)) = e^{-\bar{\alpha}L(\bar{\alpha},\mu^2)}|S(\zeta)).$$

μ is an arbitrary collinear scale, suitably chosen depending on the process (DIS, $\mu^2 = Q^2$). The L operator can be constructed to all orders in perturbation theory by imposing that the composite dipole obeys the property

$$\frac{\partial \bar{S}}{\partial \ln \zeta} = -\frac{\partial \bar{S}}{\partial \ln \mu^2}$$

which implies that

$$\bar{S}(\zeta,\mu^2) = \bar{S}(\frac{\zeta}{\mu^2}).$$

The high-energy evolution of $\bar{S}$ does not depend on μ to all orders.

Fixed coupling

$$\frac{\partial \bar{S}_{12}}{\partial Y} = \bar{\alpha} \int_{x_3} \frac{x_{12}^2}{x_{13}^2 x_{23}^2} \left[\bar{S}_{13}\bar{S}_{23} - \bar{S}_{12} \right] +$$

$$+ \bar{\alpha}^2 \int_{x_3} \frac{x_{12}^2}{x_{13}^2 x_{23}^2} \left[\frac{1}{12}\beta \left\{ \ln(x_{12}\mu_R) - \frac{x_{13}^2 - x_{23}^2}{x_{12}^2} \ln\left(\frac{x_{13}^2}{x_{23}^2}\right) \right\} + const \right] \left[\bar{S}_{13}\bar{S}_{23} - \bar{S}_{12} \right] +$$

$$+ \frac{1}{2}\bar{\alpha}^2 \int_{x_3,x_4} K_{1234} \left[\bar{S}_{13}\bar{S}_{34}\bar{S}_{42} - \bar{S}_{13}\bar{S}_{32} \right] +$$

$$+ \frac{n_f}{2N_c}\bar{\alpha}^2 \int_{x_3,x_4} K_f \left[\bar{S}_{32}\bar{S}_{14} - \bar{S}_{32}\bar{S}_{13} \right] +$$

$$+ \frac{1}{2}\bar{\alpha}^2 \int_{x_3,x_4} \frac{x_{12}^2}{x_{13}^2 x_{23}^2} \frac{x_{32}^2}{x_{34}^2 x_{24}^2} \ln\left(\frac{x_{34}^2}{x_{14}^2}\right) \left[\bar{S}_{13}\bar{S}_{34}\bar{S}_{42} - \bar{S}_{13}\bar{S}_{32} \right] +$$

$$+ \frac{1}{2}\bar{\alpha}^2 \int_{x_3,x_4} \frac{x_{12}^2}{x_{13}^2 x_{23}^2} \frac{x_{13}^2}{x_{14}^2 x_{34}^2} \ln\left(\frac{x_{34}^2}{x_{24}^2}\right) \left[\bar{S}_{14}\bar{S}_{43}\bar{S}_{32} - \bar{S}_{13}\bar{S}_{32} \right]$$

Fixed coupling

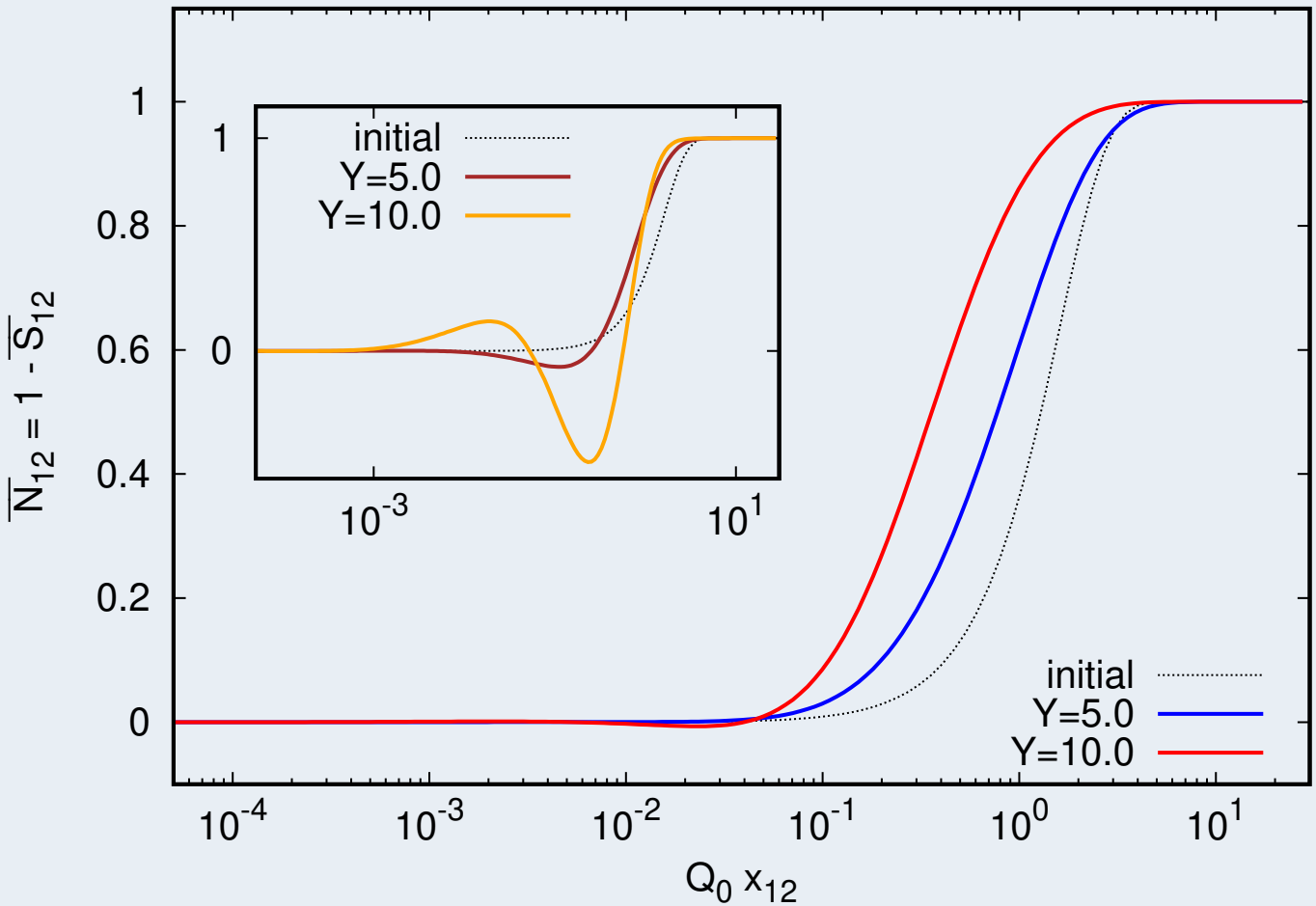

Figure: Evolution of $\bar{N}_{12}$ to $Y = 5$ (blue line) and $Y = 10$ (red line). The inset shows the evolution using the standard NLO BK equation.

Numerical setup

- the transverse area integrals on the right-hand side of the evolution equation are evaluated using polar coordinates,
- the radial variables are discretized on a logarithmic grid,
- a grid of 256 nodes for $|\boldsymbol{x}_3|$ and $|\boldsymbol{x}_4|$ on the interval $[10^{-7}, 30]$ is enough,
- the angular degrees of freedom ϕ_3 and ϕ_4 were discretized using 16 nodes,
- we employ the Simpson $\frac{3}{8}$ quadrature scheme for both the angular and the radial variables, i.e., each angular variable is sampled at 48 points.

Performance:

- CPU implementation: runs up to 48h
- GPU implementation: runs up to 4h
- GPU implementation with running coupling: runs up to 72h

Numerical setup

The choice of the coordinate systems for $\boldsymbol{x}_3$ and $\boldsymbol{x}_4$ is made such that the coordinates $\boldsymbol{x}_1$ and $\boldsymbol{x}_2$ lie along the x-axis, with the origin set at $\frac{1}{2}(\boldsymbol{x}_1 + \boldsymbol{x}_2)$. In the two integrals involved in the K_{1234} and K_f terms, the position $\boldsymbol{x}_4$ is measured with respect to the position $\boldsymbol{x}_3$. The latter choice is dictated by the fact that in such a coordinate system, one can analytically cancel the divergence $1/\boldsymbol{x}_{34}^4$ in the limit of small $\boldsymbol{x}_{12}$, which otherwise becomes numerically unstable.

We checked that increasing the resolution in the discretization of all degrees of freedom and extending the interval for the radial variables does not alter the resulting dipole. Eventually, we also tested that running the evolution in double and long double precision yields compatible results.

Numerical setup

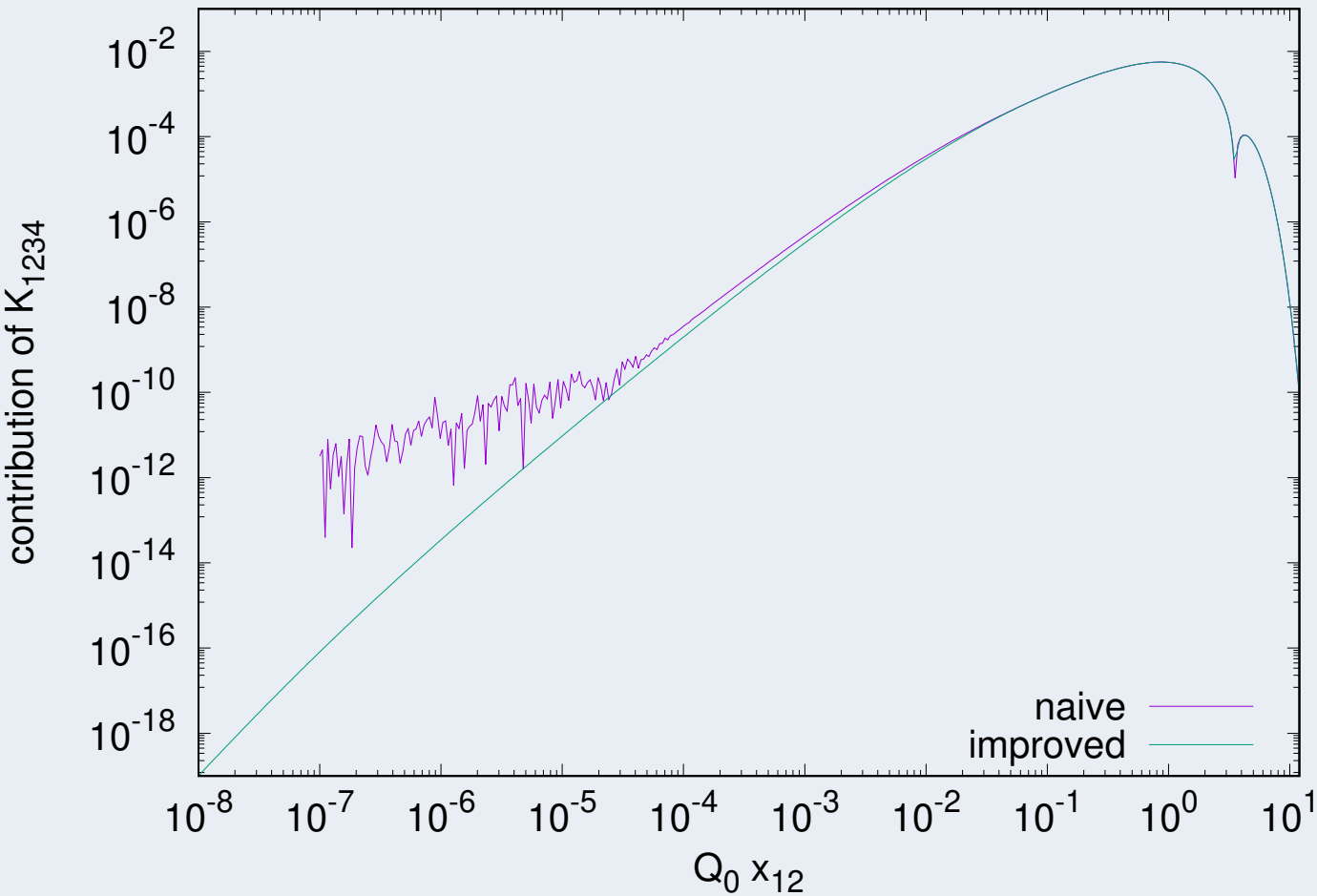

Figure: Cancellation of divergence in the K_{1234} term. This term also contains single logarithms. At fixed coupling, its impact on the evolution is negligible.

Fixed coupling

The differential equation is integrated numerically, i.e. the rapidity variable Y is discretized with some small step δ, $Y_n = Y_0 + n\delta$, and the amplitude $\bar{S}_{12}(Y_{n+1} = Y_n + \delta)$ is obtained from its previous state $\bar{S}_{12}(Y_n)$ using one of the three integration rules: Euler, Heun, or midpoint. The Euler method advances the solution through

$$\bar{S}_{12}(Y_{n+1}) = \bar{S}_{12}(Y_n) + \delta f(\ \bar{S}_{12}(Y_n)\ ),$$

the Heun method through

$$\bar{S}_{12}(Y_{n+1}) = \bar{S}_{12}(Y_n) + \frac{\delta}{2}\left\{f(\ \bar{S}_{12}(Y_n)\ ) + f\left[\bar{S}_{12}(Y_n) + \delta f(\ \bar{S}_{12}(Y_n)\ )\right]\right\},$$

whereas the midpoint method uses

$$\bar{S}_{12}(Y_{n+1}) = \bar{S}_{12}(Y_n) + \delta f\left[\bar{S}_{12}(Y_n) + \frac{\delta}{2} f(\ \bar{S}_{12}(Y_n)\ )\right].$$

Fixed coupling

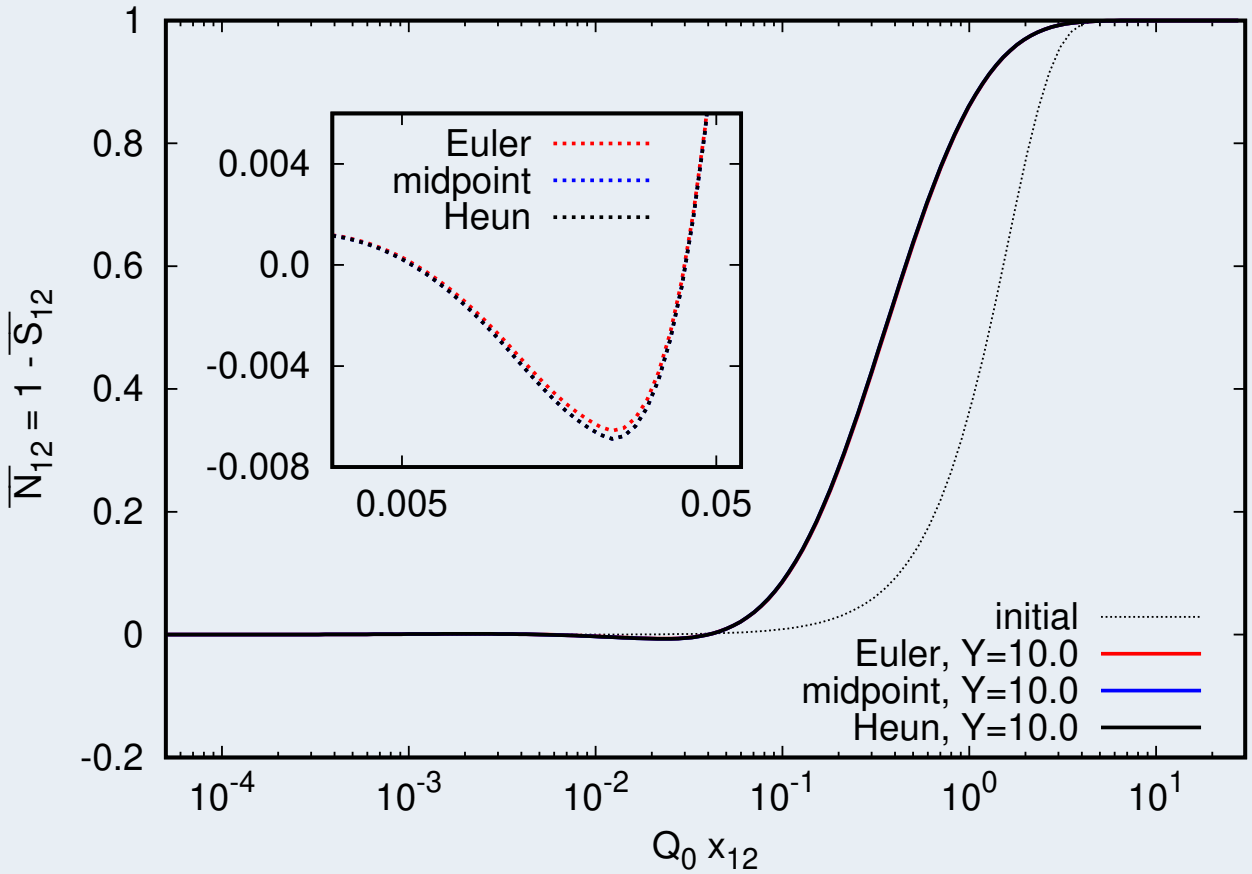

Figure: The evolution of $\bar{N}_{12}$ up to $Y = 10.0$ with $N = 256$. The black dashed curve denotes the initial condition, while the colored data correspond to different integration schemes.

Fixed coupling

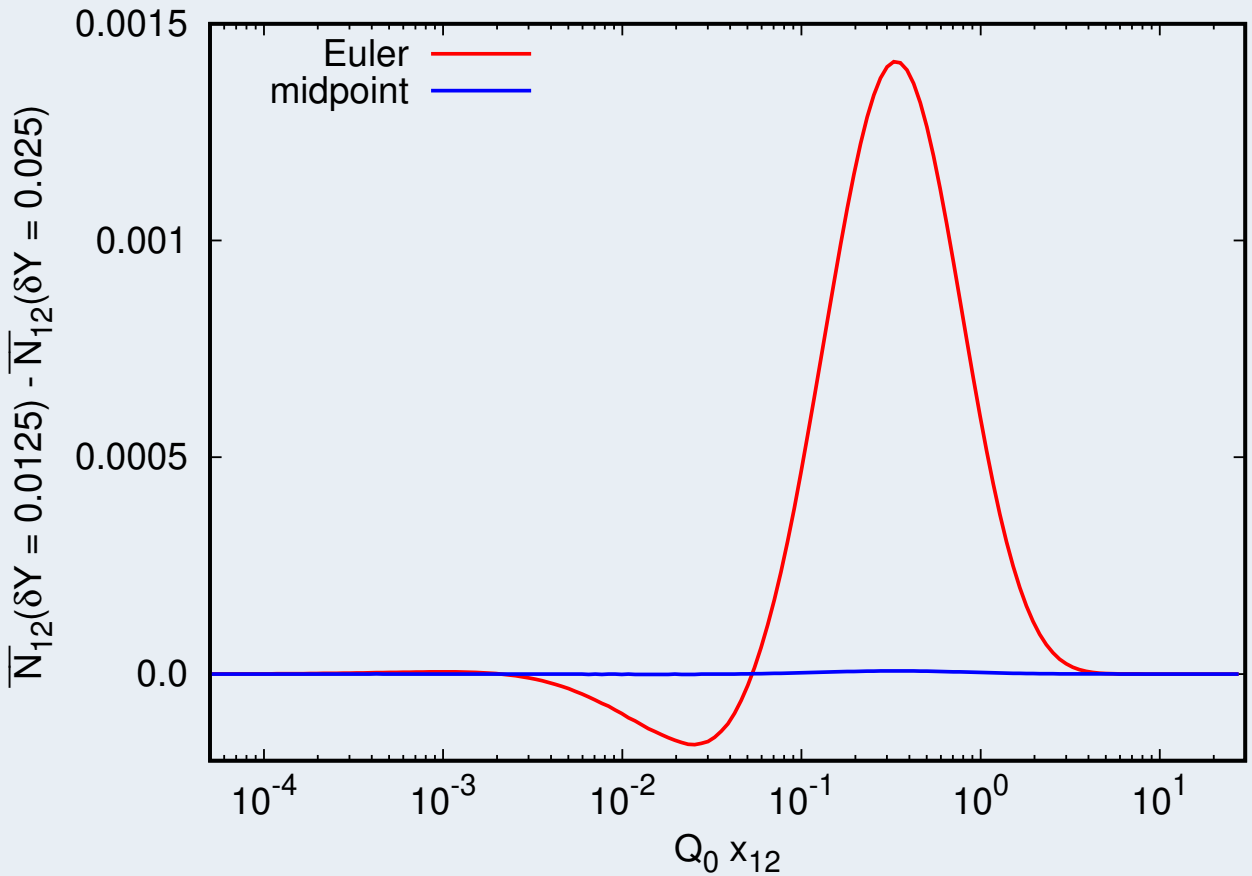

Figure: The evolution of $\bar{N}_{12}$ up to $Y = 10.0$ with $N = 256$. Plotted is the difference between the results obtained with $\delta Y = 0.025$ and $\delta Y = 0.0125$.

Fixed coupling

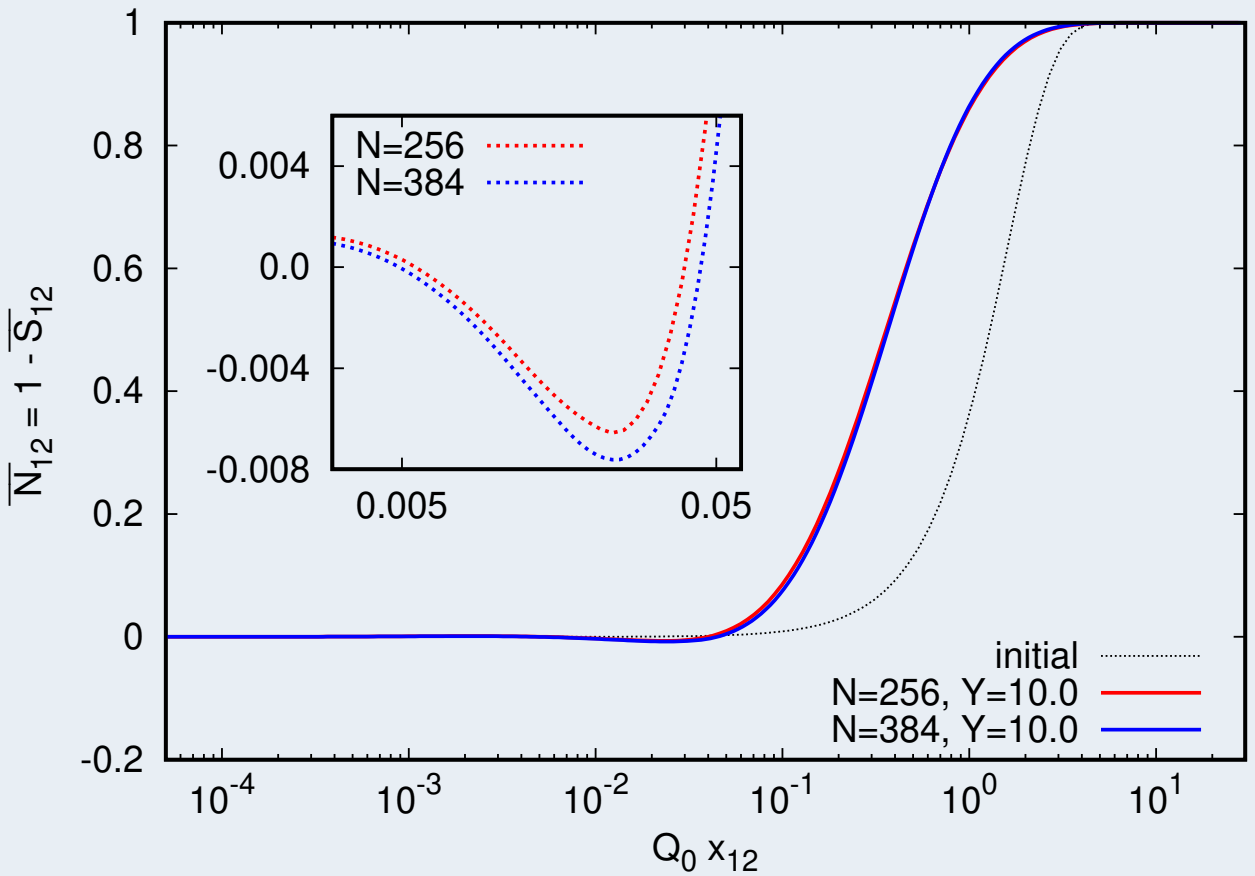

Figure: The evolution of $\bar{N}_{12}$ from the initial condition up to $Y = 10.0$ using the Euler method and two different grid sizes: red: $N = 256$ and blue: $N = 384$.

Fixed coupling

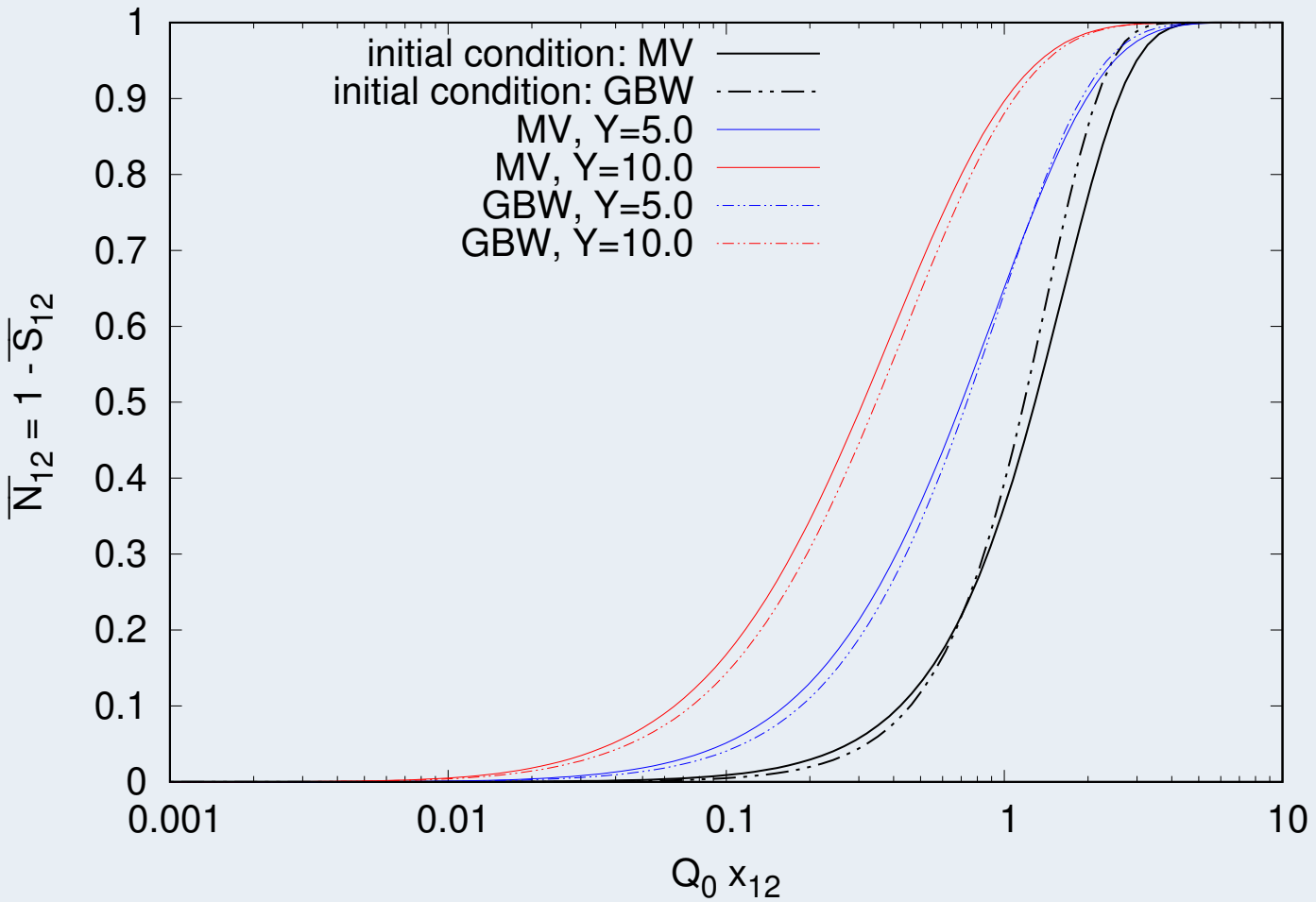

Figure: Comparison of evolutions at NLO for different initial conditions: GBW and MV.

Fixed coupling

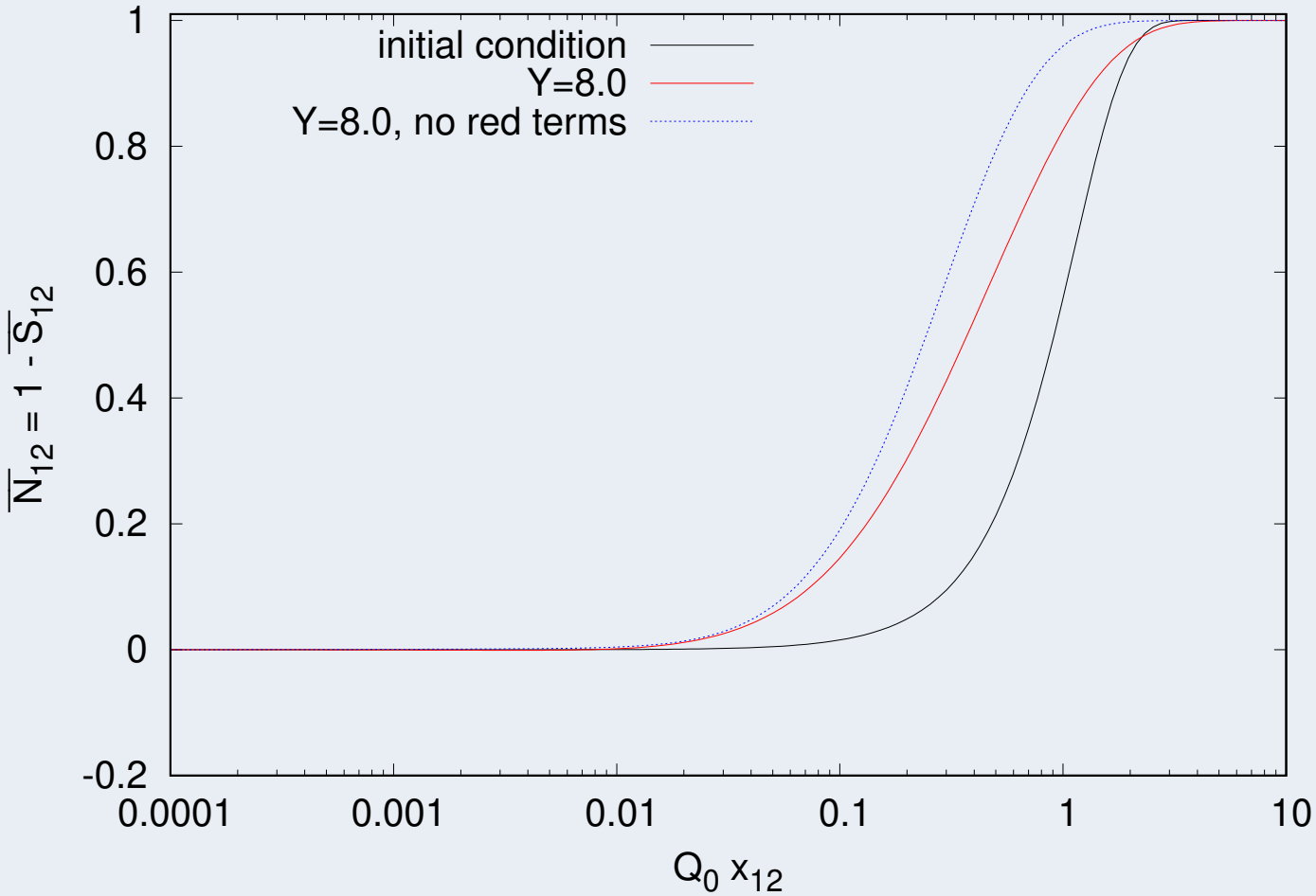

Figure: Comparison of evolutions at NLO with and without the red terms. They contain anti-collinear logarithms.

Running coupling: preliminary

Full equation with running coupling constant, BLM prescription, and $\mu_{123} = \mu_R$:

$$\frac{\partial \bar{S}_{12}}{\partial Y} = \int_{x_3} \bar{\alpha}(\mu_{123}) \frac{x_{12}^2}{x_{13}^2 x_{23}^2} \left[\bar{S}_{13}\bar{S}_{23} - \bar{S}_{12}\right] +$$

$$+ \int_{x_3} \bar{\alpha}^2(\mu_{123}) \frac{x_{12}^2}{x_{13}^2 x_{23}^2} \left[\frac{1}{12}\beta \left\{ \ln(x_{12}\mu_R) - \frac{x_{13}^2 - x_{23}^2}{x_{12}^2} \ln\left(\frac{x_{13}^2}{x_{23}^2}\right)\right\} + \right.$$

$$\left. + const \right] \left[\bar{S}_{13}\bar{S}_{23} - \bar{S}_{12}\right] +$$

$$+ \frac{1}{2}\int_{x_3,x_4} \bar{\alpha}^2(\mu_{1234}) K_{1234} \left[\bar{S}_{13}\bar{S}_{34}\bar{S}_{42} - \bar{S}_{13}\bar{S}_{32}\right] +$$

$$+ \frac{n_f}{2N_c}\int_{x_3,x_4} \bar{\alpha}^2(\mu_{1234f}) K_f \left[\bar{S}_{32}\bar{S}_{14} - \bar{S}_{32}\bar{S}_{13}\right] +$$

$$+ \frac{1}{2}\int_{x_3,x_4} \bar{\alpha}(\mu_{123})\bar{\alpha}(\mu_{324}) \frac{x_{12}^2}{x_{13}^2 x_{23}^2} \frac{x_{32}^2}{x_{34}^2 x_{24}^2} \ln\left(\frac{x_{34}^2}{x_{14}^2}\right) \left[\bar{S}_{13}\bar{S}_{34}\bar{S}_{42} - \bar{S}_{13}\bar{S}_{32}\right] +$$

$$+ \frac{1}{2}\int_{x_3,x_4} \bar{\alpha}(\mu_{123})\bar{\alpha}(\mu_{134}) \frac{x_{12}^2}{x_{13}^2 x_{23}^2} \frac{x_{13}^2}{x_{14}^2 x_{34}^2} \ln\left(\frac{x_{34}^2}{x_{24}^2}\right) \left[\bar{S}_{14}\bar{S}_{43}\bar{S}_{32} - \bar{S}_{13}\bar{S}_{32}\right] + \ldots$$

Running coupling: preliminary

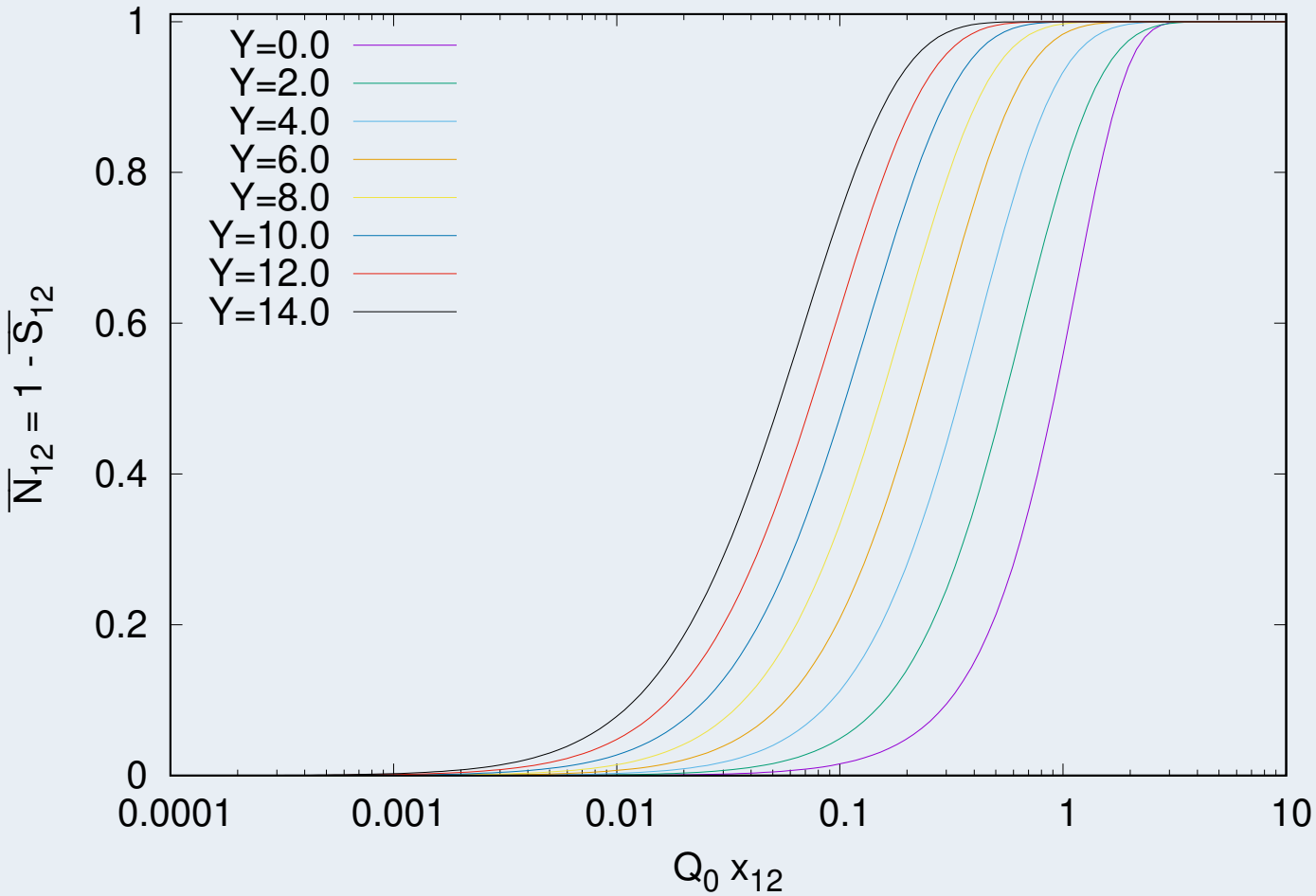

Figure: Evolution at NLO with running coupling in the BLM prescription with the first part of the equation. μ_{1234} and μ_{1234f} kept fixed.

Running coupling: preliminary

$$
\begin{aligned}
\frac{\partial \bar{S}_{12}}{\partial Y} = & \ldots \\
& + \frac{1}{2}\int_{x_3,x_4} \left(\bar{\alpha}(\mu_{124})\bar{\alpha}(\mu_{143}) - \bar{\alpha}(\mu_{123})\bar{\alpha}(\mu_{324})\right) \frac{x_{12}^2}{x_{13}^2 x_{34}^2 x_{24}^2} \times \\
& \times \ln\left(\frac{x_{13}^2 x_{32}^2}{x_{14}^2 x_{42}^2}\right)\left[\bar{S}_{13}\bar{S}_{34}\bar{S}_{42} - \bar{S}_{13}\bar{S}_{32}\right] + \\
& + \frac{1}{2}\int_{x_3,x_4} \Bigg[\left(\bar{\alpha}(\mu_{123})\bar{\alpha}(\mu_{134}) - \bar{\alpha}(\mu_{123})\bar{\alpha}(\mu_{123})\right) \frac{x_{12}^2}{x_{14}^2 x_{34}^2 x_{23}^2} + \\
& - \left(\bar{\alpha}(\mu_{123})\bar{\alpha}(\mu_{124}) - \bar{\alpha}(\mu_{123})\bar{\alpha}(\mu_{123})\right) \frac{x_{12}^2 x_{12}^2}{x_{13}^2 x_{14}^2 x_{34}^2 x_{23}^2} + \\
& + \left(\bar{\alpha}(\mu_{123})\bar{\alpha}(\mu_{143}) + \bar{\alpha}(\mu_{123})\bar{\alpha}(\mu_{124}) - 2\bar{\alpha}(\mu_{123})\bar{\alpha}(\mu_{123})\right) \frac{x_{12}^2}{x_{13}^2 x_{34}^2 x_{24}^2} + \\
& + \left(\bar{\alpha}(\mu_{124}) - \bar{\alpha}(\mu_{123})\right)\left(\bar{\alpha}(\mu_{143}) - \bar{\alpha}(\mu_{123})\right) \frac{x_{12}^2}{x_{13}^2 x_{34}^2 x_{24}^2} \\
& \Bigg] \ln\left(\frac{x_{13}^2 x_{32}^2}{x_{14}^2 x_{42}^2}\right)\left[\bar{S}_{13}\bar{S}_{32} - \bar{S}_{12}\right]
\end{aligned}
$$

Running coupling: preliminary

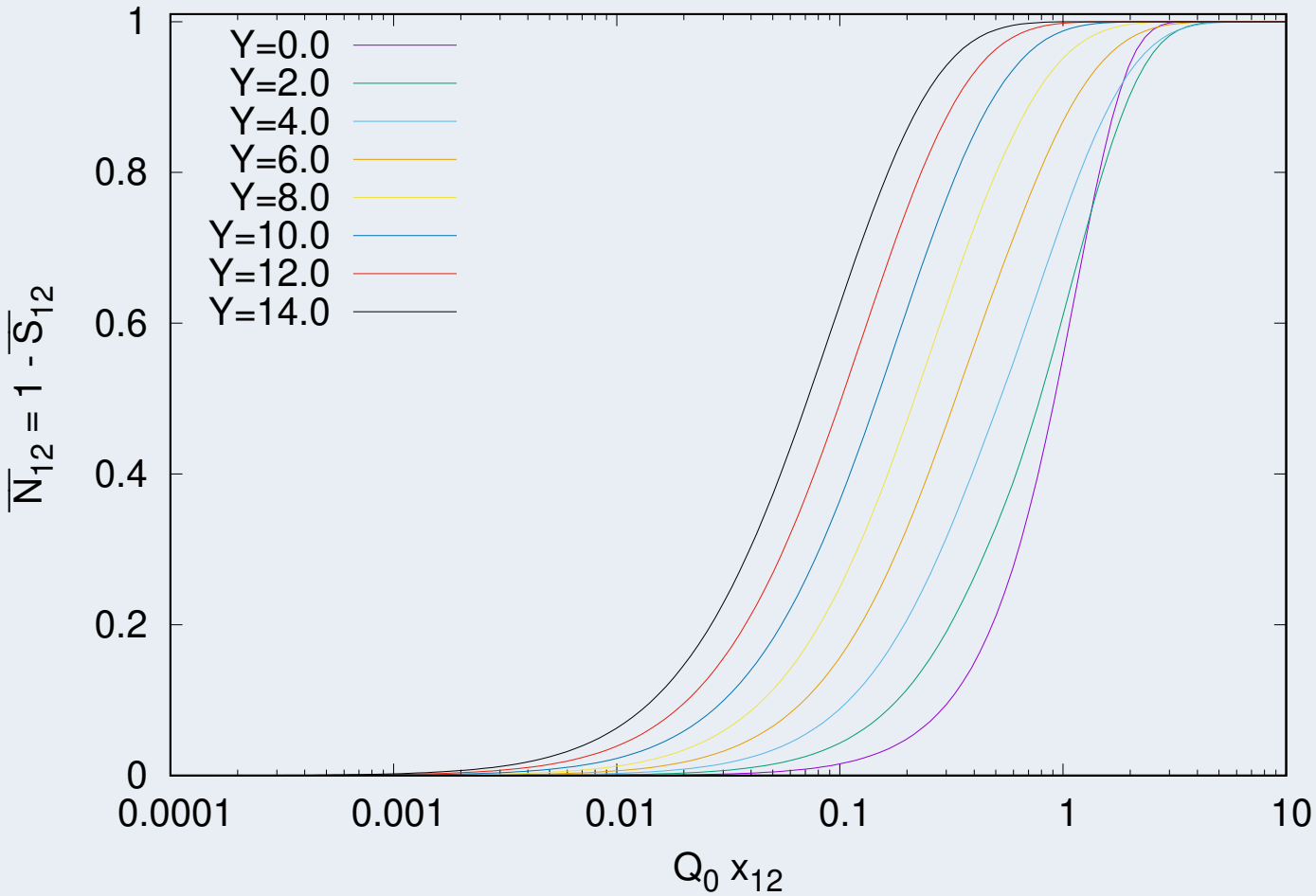

Figure: Evolution at NLO with running coupling in the BLM prescription with the full equation. μ_{1234} and μ_{1234f} kept fixed.

Running coupling: preliminary

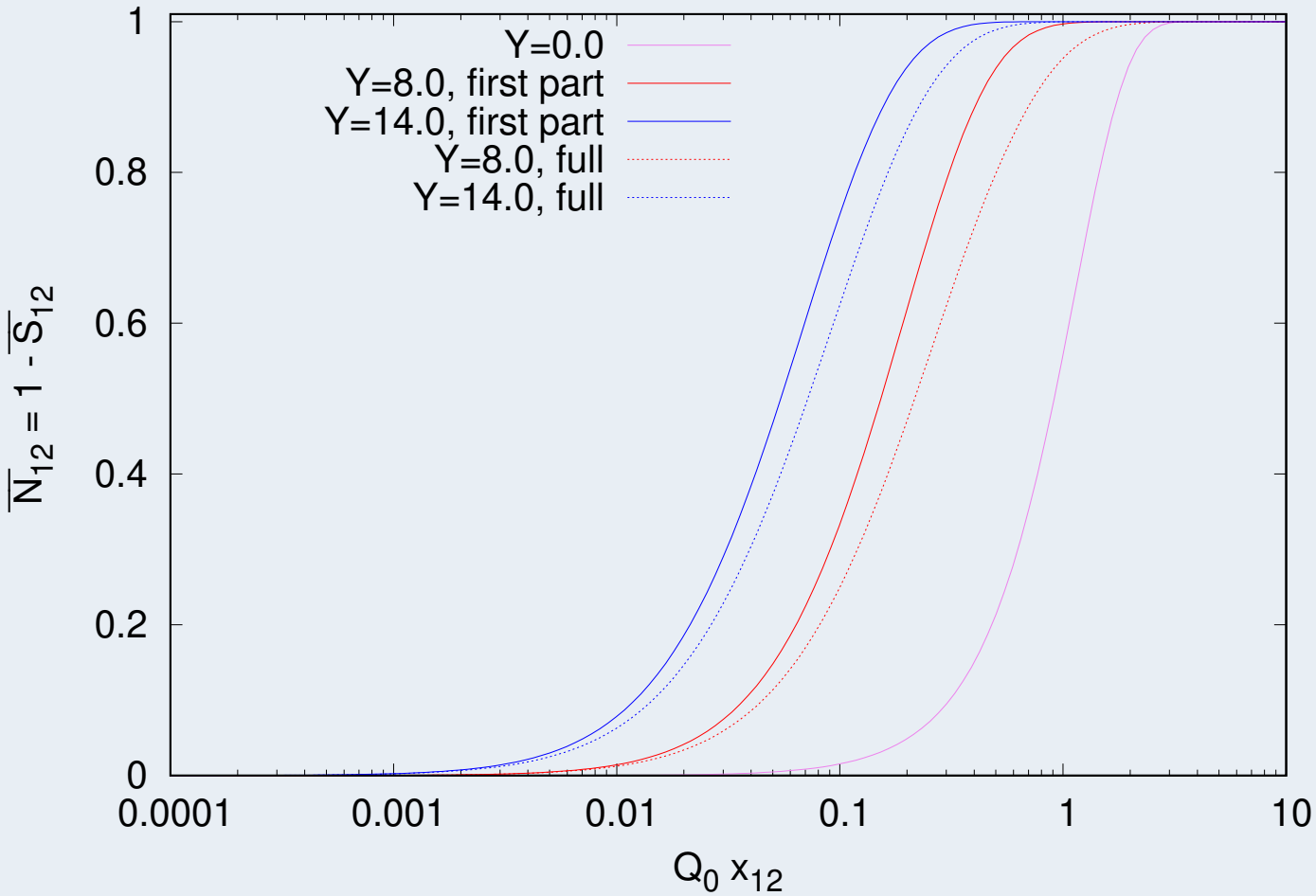

Figure: Comparison of evolutions at NLO with running coupling in the BLM prescription. μ_{1234} and μ_{1234f} kept fixed.

NLO approach to BK

Summary

- efficient and stable implementation of the NLO BK equation for the rotated dipole;
- we see stable evolution at fixed coupling up to very high Y;
- preliminary: stable evolution with BLM prescription for the running coupling; K_{1234} and K_f at fixed coupling; sensitive to the prescription;

Outlook

- combine with DIS NLO form factor and calculate NLO DIS cross-sections

Acknowledgments for computing grants

- We gratefully acknowledge Polish high-performance computing infrastructure PLGrid (HPC Center: ACK Cyfronet AGH) for providing computer facilities and support within computational grant no. PLG/2024/017690.
- We acknowledge Polish high-performance computing infrastructure PLGrid for awarding this project access to the LUMI supercomputer, owned by the EuroHPC Joint Undertaking, hosted by CSC (Finland) and the LUMI consortium through PLL/2025/08/018112